Stark structure in Rydberg states of xenon

R. D. Knight and Liang-guo Wang
Department of Physics, The Ohio State University, Columbus, Ohio 43210-1106
(Received 29 March 1985)

We have studied the Stark effect for the bound Rydberg states of xenon ($^2P_{3/2}$ core) in the vicinity of $n=17$. These are the first detailed measurements of Rydberg-state Stark structure in a heavy rare-gas atom. The experiment was performed by one-photon laser spectroscopy from the metastable $6s'[\frac{1}{2}]_0$ state in an atomic beam. Laser polarization can be chosen to excite pure $M=0$ or $|M|=1$ levels. Stark maps are presented for electric fields from 0 to 2000 V/cm. The major low-field features are a prominent linear manifold for states with $l \geq 3$ and an isolated group of states arising from mixing within the overlapping p and d terms. A simple model of the p,d complex, showing strong mixing at fields as low as 200 V/cm, is used to correlate observed states with the zero-field states. The spectra become exceedingly complex for fields greater than 1000 V/cm because of mixing within the extensive fine structure of xenon.

I. INTRODUCTION

Rydberg states of the rare gases have received considerably less attention than the highly excited states of alkali-metal and alkaline-earth atoms, despite the fact that multichannel quantum-defect theory was motivated largely by attempts to understand their highly excited and autoionizing levels. This situation is due, in large part, to the experimental difficulties of performing high-resolution spectroscopy on the excited states of the rare gases. Recently, however, the techniques of metastable beam spectroscopy[1–3] and optogalvanic spectroscopy[4,5] have been applied by an increasing number of investigators to studies of the Rydberg states of the rare gases.

The structure of a Rydberg-state rare-gas atom differs in significant details from that of an alkali-metal or alkaline-earth atom. First, the presence of fine structure in the ionic core leads to overlapping Rydberg series converging to each ionization limit and thus to singly excited autoionizing levels. Second, the fine structure of the rare gases is extremely complex. Only a few studies have yet addressed the question of how these details affect the Stark structure of Rydberg-state rare-gas atoms. Low-resolution vuv measurements have been used to study the effect of electric fields on autoionization resonances in xenon,[6] and laser investigations in krypton have probed field-induced resonances in the photoionization continuum[7] and the Stark structure of autoionizing Rydberg series converging to the second ionization limit.[8] To our knowledge there has been no theoretical work for electric field effects on the Rydberg states of the heavy rare gases, although a perturbation calculation for low-lying levels of argon was successfully undertaken over 30 years ago.[9]

Recently Harmin[10] has developed a semianalytical treatment of the Stark effect based on quantum-defect theory. His treatment separates the problem into an inner region, in which the external field is negligible in comparison with the Coulomb field, and an outer region, which is well characterized by the hydrogenic Stark effect. His theory provides an excellent description of the observed Stark effect in Rydberg-state Li (Ref. 10) and has also successfully been applied to a detailed study of the ionization of highly excited He (Ref. 11). Further extensions of this theory are needed before it can address the problem of Stark structure in the heavy rare gases, and we hope that our findings will motivate further efforts.

In this paper we report the results of Stark-structure measurements in the vicinity of the $n=17$ states of the lowest Rydberg series of xenon ($^2P_{3/2}$ core). These are the first detailed measurements of the Stark effect in the bound Rydberg states of a heavy rare-gas atom. Xenon was chosen for these measurements for several reasons. First, one-photon laser spectroscopy of the Rydberg states is conveniently performed from the metastable $6s'[\frac{1}{2}]_0$ state. Second, the $M=0$ character of the initial state allows pure $M=0$ or $|M|=1$ manifolds to be excited, greatly simplifying the task of analysis. Such was not the case for the laser investigations of Kr cited above.[7,8] Third, no resonance levels with a $^2P_{1/2}$ core are located near the $^2P_{3/2}$ ionization limit, thus eliminating possibly serious perturbations. Xenon, then, should be a valuable choice for studying the essential features of the Stark effect in the rare gases.

Our method has been to obtain Stark maps for xenon in a narrow region around $n=17$ for field strengths up to 2000 V/cm. Our work can thus be viewed as a direct extension of the earlier work of Zimmerman *et al.* on the Stark structure of alkali-metal atoms[12] and barium.[13] It will be seen that the extensive fine structure of xenon leads to Stark maps more complex than those of Zimmerman *et al.*, and that a complete analysis is not feasible at this time. We nonetheless are able to identify the major features of the spectra, and a partial analysis of the low-field behavior within the p,d complex will be presented in Sec. IV.

II. EXPERIMENTAL PROCEDURE

The experiment has been described elsewhere[3] and will only be summarized here. A metastable xenon beam is

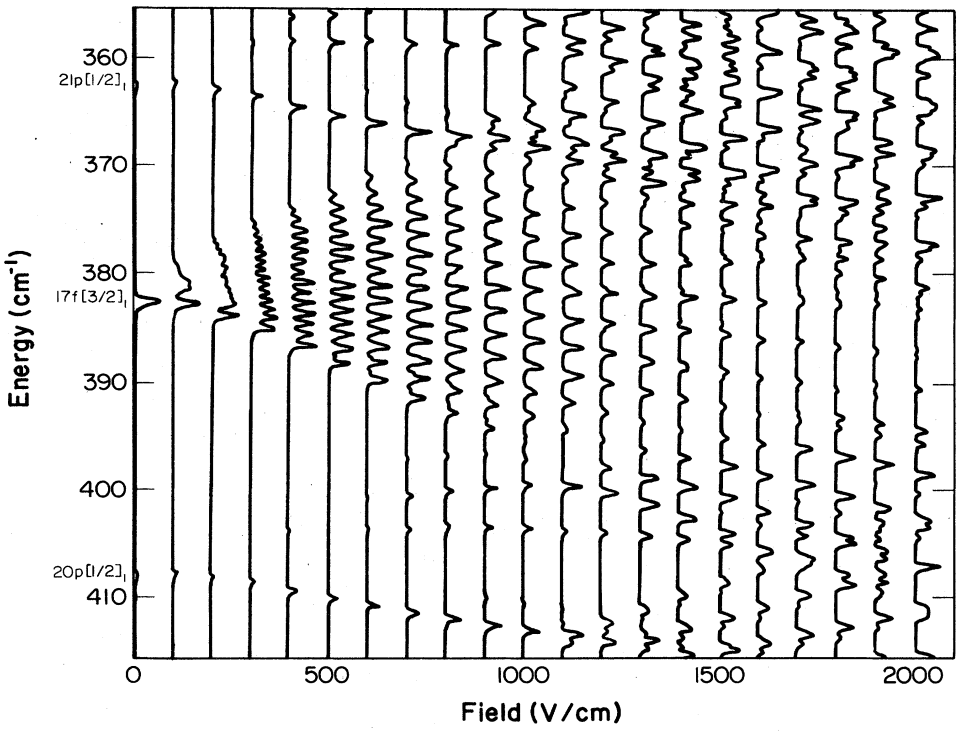

FIG. 1. Stark map for the $M=0$ states of xenon near $n=17$.

formed by electron impact on gas flowing from an effusive nozzle. Both the $6s'[\frac{1}{2}]_0$ and $6s[\frac{3}{2}]_2$ metastable states are populated, but only the $J=0$ state was used for the measurements reported here. The atomic beam passed through a parallel-plate interaction region where it was intersected at right angles by the unfocused beam of a neodymium—yttrium-aluminum-garnet (Nd:YAG)-pumped dye laser. A dc electric field up to 2000 V/cm could be applied to the interaction region, and a high-voltage pulse immediately following the laser was then used to field ionize Rydberg atoms. Resulting electrons were detected by a Channeltron detector and the signal averaged with a boxcar integrator.

In the zero-field spectrum, which we have described elsewhere,[3] the most prominent Rydberg series is $6s'[\frac{1}{2}]_0$-$nf[\frac{3}{2}]_1$. Also present, although weak, is $6s'[\frac{1}{2}]_0$-$np[\frac{1}{2}]_1$. The $6s'[\frac{1}{2}]_0$-$np[\frac{3}{2}]_1$ series, which might be expected, is not seen. For the Stark measurements, we repeatedly scanned the laser ($\lambda\approx 470$ nm) over the $20p$-$17f$-$21p$ region as the dc field was increased. A Fabry-Perot etalon monitoring the laser indicated a laser linewidth ≈ 0.3 cm^{-1} and a scan reproducibility of ± 0.1 cm^{-1}. The laser polarization could be rotated to be either parallel ($\Delta M=0$ transitions) or perpendicular ($\Delta M=\pm 1$ transitions) to the dc electric field.

III. RESULTS

Since we start from an $M=0$ level, the $\Delta M=0$ and $\Delta M=\pm 1$ transitions excite pure $M=0$ and $|M|=1$ Stark manifolds. As has become customary for the study of Stark structure in Rydberg states, we find it easiest and most useful to present our results as Stark maps. Figure 1 shows the Stark map of the $M=0$ manifold in the region near $n=17$, with data presented every 100 V/cm up to 2000 V/cm. The $|M|=1$ manifold does not differ in any significant fashion and will not be presented here. The maps give a reliable indication as to energy-level positions, but they should not be considered as more than a rough guide as to intensities. This is due to the fact that Channeltron detectors are not highly linear, the laser power was only approximately constant throughout a run, and the data were normalized to give the same maximum peak height in each scan before plotting.

The observed spectra show more complexity than do those for Li or Cs (Ref. 12), even though Cs and Xe are adjacent in the Periodic Table. This complexity results

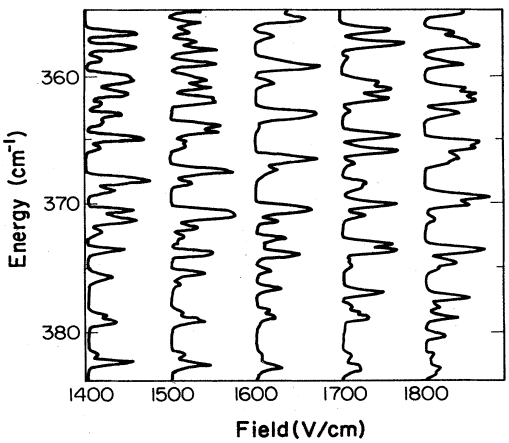

FIG. 2. Enlarged section of the Stark map shown in Fig. 1.

from the extensive fine structure of xenon, a matter to be discussed in Sec. IV. Many of the measurable details are not apparent in the reduction necessary for Fig. 1. An enlarged section of the Stark map is shown in Fig. 2 to give a better idea of the details. In addition, enlargements show that numerous small peaks are to be found between the p states and the main manifold for fields $\gtrsim 200$ V/cm. They do not become visible in Fig. 1 until fields $\gtrsim 400$ V/cm. These peaks are due to interactions within the p,d complex and will be discussed in Sec. IV.

IV. DISCUSSION

The most prominent feature of these spectra is the linear manifold, composed of the essentially degenerate $l=4$–16 states with the $l=3$, f state having merged by 400 V/cm. The $17f[\frac{3}{2}]_1$ state has only a small quantum defect,[3] $\mu=0.0560$, and so interacts strongly with the g state and thus the entire degenerate manifold. Since the transitions to $nf[\frac{3}{2}]_1$ are the strongest of the zero-field transitions, the linear manifold achieves considerable intensity even at very low-field strengths. This is in contrast to the situation in cesium,[12] where the linear manifold is not seen for low-field strengths. In that case, all zero-field intensity is concentrated in the s-p transitions, and both p and d states are well removed from the manifold. Only for large fields does p character mix, via the d states, into the linear manifold.

By an interesting coincidence, the $21s[\frac{3}{2}]_{1,2}$ states are essentially degenerate with the linear manifold,[5] having quantum defects $\mu=3.991$ and 4.021, respectively. The linear manifold is observed, however, to consist of only 14 equally spaced peaks, corresponding to $l=3$–16, indicating that the two s states are not being seen. The reason is not hard to discern. To have measurable intensity in transitions from the initial $6s'[\frac{1}{2}]_0$ state, the $21s[\frac{3}{2}]_{1,2}$ states must acquire either $p[\frac{1}{2},\frac{3}{2}]_1$ character or $f[\frac{3}{2}]_1$ character. Neither is likely at low fields, since the p states are too far away while the nearby $17f[\frac{3}{2}]_1$ state will mix with $21s[\frac{3}{2}]_{1,2}$ only through a higher-order $\Delta l=3$ process. An additional consideration is that the s states are located almost exactly halfway between the $20p$ and $21p$ states. Thus the repulsions from the p states will nearly cancel and we would expect the s states to remain at nearly constant energy up to large field strengths. Once this behavior is predicted, likely evidence of the presence of the s states can be seen in the recurring dip in intensity at the center of the linear manifold ($\mu=0$) and in the fact that splitting of the manifold peaks into more complex structures, as the interaction energy increases, begins near $\mu=0$ for a field ≈ 1100 V/cm.

Besides the linear manifold, one observes a variety of seemingly isolated small peaks, including the $20,21p[\frac{3}{2}]_1$ peaks seen at zero field, which gradually merge with the linear manifold for $E>1000$ V/cm. As noted previously, enlargement of the spectra show these peaks for fields $\gtrsim 200$ V/cm. These peaks are associated with the p and d terms, both of which exhibit extensive and overlapping fine structure throughout the regions between the linear manifolds. Because of the overlapping, these states will be strongly mixed even at low fields, and consequently one cannot hope to determine the correlation of observed peaks with zero-field states without some more quantitative analysis.

The p,d complex itself consists of 14 fine-structure components, while the entire $n=17$ term is comprised of 128 components having $M=0$ levels. A comprehensive matrix-diagonalization procedure, such as Zimmerman *et al.* carried out for the alkali-metals,[12] would need to include at least $n=15$–19 to allow for interactions between neighboring Rydberg states. This requires a minimum of 640 basis states, and so the computational effort would be immense. Rather than attempt to analyze the general situation, we have chosen to analyze the $19d,20p$ complex in isolation. Since the p,d complexes are reasonably well separated at zero field from all other states, our model is expected to be adequate for determining the low-field mixing. In particular, the goal of this model is to correlate the observed states with the appropriate zero-field states to which they join adiabatically. This model clearly breaks down as the p and d states begin to merge with the linear manifold. We will deal specifically with the $M=0$ manifold of the $19d,20p$ complex.

The heavy rare gases are generally described best by the jl coupling scheme, although even this scheme has serious deficiencies.[3] In jl coupling the orbital angular momentum l of the excited electron is strongly coupled to the angular momentum j of the core ($j=\frac{1}{2},\frac{3}{2}$) to produce a resultant angular momentum K. K is then weakly coupled to the excited electron spin S ($S=\frac{1}{2}$), giving the total angular momentum J. Notation is $nl[K]_J$, with a prime on l indicating $j=\frac{1}{2}$.

The Stark Hamiltonian is given by $H_{\text{Stark}}=eEz$. Although we are only considering weak fields, the p and d states are so thoroughly mixed that one must proceed by diagonalization of the entire matrix, $H=H_0+eEz$, rather than by perturbation theory. The diagonal matrix elements are just the zero-field energies, which have measured values for the d states[5] and can be inferred to sufficient precision from quantum defects for the p states. One state in particular, $19d[\frac{3}{2}]_1$, is noted to be far removed from its fine-structure partner, $19d[\frac{3}{2}]_2$, indicating a breakdown of the jl coupling approximation.

Computation of the off-diagonal matrix elements in jl coupling is the heart of the calculation. Parity considerations dictate $\Delta l=1$ for the matrix elements, so there are no elements connecting states within the same term. For the general p-d matrix element, the Wigner-Eckart theorem gives

$$\langle(\nu lj)KSJM\,|\,z\,|\,(\nu' l' j')K'S'J'M'\rangle = (-1)^{J-M}\begin{pmatrix} J & 1 & J' \\ -M & 0 & M' \end{pmatrix} \times\langle(\nu lj)KSJ||\mathbf{r}||(\nu' l' j')K'S'J'\rangle\ . \quad (1)$$

The effective quantum number ν is used, rather than n, in anticipation of its need when evaluating radial integrals. Standard angular momentum algebra provides simplification of the reduced matrix element:

$$\langle (\nu lj)KSJ||\mathbf{r}||(\nu' l' j')K'S'J'\rangle = (-1)^{K+S+J'+1}[(2J+1)(2J'+1)]^{1/2} \times \begin{Bmatrix} K & J & S \\ J' & K' & 1 \end{Bmatrix} \delta_{SS'} \langle (\nu l)jK||\mathbf{r}||(\nu' l')j'K'\rangle \quad (2)$$

followed by

$$\langle (\nu l)jK||\mathbf{r}||(\nu' l')j'K'\rangle = (-1)^{l+j+K'+1}[(2K+1)(2K'+1)]^{1/2} \times \begin{Bmatrix} l & K & j \\ K' & l' & 1 \end{Bmatrix} \delta_{jj'} \langle \nu l||\mathbf{r}||\nu' l'\rangle \ . \quad (3)$$

From the Kronecker deltas and the 3-j and 6-j symbols follow the usual selection rules in jl coupling:

$$\Delta M = \Delta S = \Delta j = 0 \ , \quad \Delta J = 0, \pm 1 \ , \quad \Delta K = 0, \pm 1 \ , \quad \Delta l = \pm 1 \ . \quad (4)$$

Taking these into account, the nonzero matrix elements are

$$\langle (\nu lj)KSJM \mid z \mid (\nu' l' j)K'SJ'M\rangle = (-1)^{J+J'+K+K'+l+j+S-M}[(2J+1)(2J'+1)(2K+1)(2K'+1)]^{1/2} \times \begin{bmatrix} J & 1 & J' \\ -M & 0 & M \end{bmatrix} \begin{Bmatrix} K & J & S \\ J' & K' & 1 \end{Bmatrix} \begin{Bmatrix} l & K & j \\ K' & l' & 1 \end{Bmatrix} \langle \nu l||r||\nu' l'\rangle \ . \quad (5)$$

The problem is now to evaluate the reduced matrix element. The one-electron matrix element is

$$\langle \nu lm \mid z \mid \nu' l' m\rangle = \langle \nu l \mid r \mid \nu' l'\rangle \langle lm \mid \cos\theta \mid l' m\rangle \ . \quad (6)$$

But also,

$$\langle \nu lm \mid z \mid \nu' l' m\rangle = (-1)^{l-m} \begin{bmatrix} l & 1 & l' \\ -m & 0 & m \end{bmatrix} \langle \nu l||\mathbf{r}||\nu' l'\rangle \ . \quad (7)$$

Equating and setting $m=0$ gives

$$\langle \nu l||\mathbf{r}||\nu' l'\rangle = \frac{(-1)^l \langle l0 \mid \cos\theta \mid l'0\rangle}{\begin{bmatrix} l & 1 & l' \\ 0 & 0 & 0 \end{bmatrix}} \langle \nu l \mid r \mid \nu' l'\rangle \ . \quad (8)$$

The angular integral and 3-j symbol are easily evaluated, leading to

$$\langle \nu l||\mathbf{r}||\nu' l'\rangle = \begin{cases} -\sqrt{l+1}\langle \nu l \mid r \mid \nu' l+1\rangle, & l'=l+1 \\ \sqrt{l}\,\langle \nu l \mid r \mid \nu' l-1\rangle, & l'=l-1. \end{cases} \quad (9)$$

The same result can be obtained from the dotted matrix elements $\langle \nu l \vdots \mathbf{r} \vdots \nu l\rangle$ given by Condon and Shortley.[14]

Finally, we use the tables of Edmonds *et al.*[15] for evaluating the radial integral in the Coulomb approximation. Since both ν and ν' are large, their method should be accurate to much better than 0.1%, more than adequate in the present approximation. We find that $\langle 20p \mid r \mid 19d\rangle = 400$ a.u. to within 1% for all of the various fine-structure components.

From Eqs. (5) and (9), and the calculated radial integrals, we evaluated all nonzero matrix elements for the $M=0$ case. The complete Hamiltonian matrix (14×14) was then numerically diagonalized for values of E ranging from 0 to 1000 V/cm. The model is expected to break down completely by 1000 V/cm as the p and d states begin to merge with the linear manifolds. Figure 3 shows the result of the diagonalization procedure and the experi-

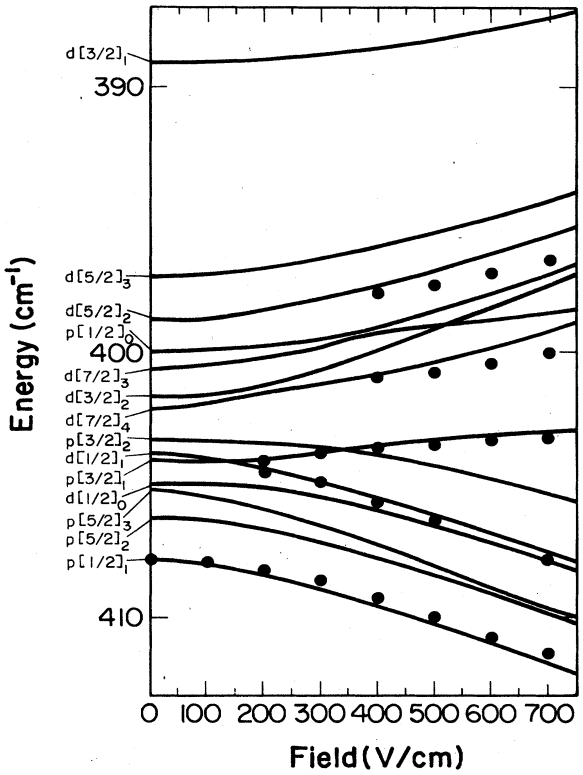

FIG. 3. Comparison of observed line positions (dots) with a low-field calculation of Stark mixing within the overlapping $19d, 20p$ levels (solid lines).

mentally observed levels. The probable error in energy of the measurements is roughly the size of the dots. It should be noted that there are no adjustable parameters in the calculation.

One discovers from this calculation that the levels of the p,d complex are indeed strongly mixed, even at low fields. Numerous avoided crossings are observed, including ones which comes too close to resolve on this scale as well as some very wide separations, such as between $d[\frac{3}{2}]_2$ and $d[\frac{7}{2}]_4$ near 150 V/cm.

Although the agreement between theory and experiment is only modest, as to be expected for such a limited model, it does improve as $E \rightarrow 0$. Thus this calculation does satisfy our goal of determining the correlation between zero-field states and the observed states. A more comprehensive calculation might be expected to reduce slightly the curvature of the levels, especially those near the edges of the complex, as they feel repulsion from states to either side of the complex. The $19d[\frac{3}{2}]_1$ state, which is rather remote from the rest of the complex, would be rather strongly repelled by the $17f$ state and might very well show almost no shift for small fields. Some evidence of this behavior can be found in the fact that the edge of the linear manifold, which correlates with the zero-field $17f$ state, begins to show complex structure at $E \approx 500$ V/cm, a field just sufficient to shift it to the $19d[\frac{3}{2}]_1$ zero-field position.

For fields $E \gtrsim 1000$ V/cm all of the fine-structure components have become so mixed as to produce a spectrum of great complexity, as observed. For fields just slightly higher, the manifolds of different n begin to cross, adding to the confusion. Our simple model is clearly inadequate for this situation, but applying the diagonalization procedure to a sufficiently large basis set seems an overly burdensome process for such a physically simple problem. An extension of Harmin's quantum-defect theory[10] of the Stark effect to the rare-gas atoms would be a welcome development.

V. CONCLUSION

We have studied the Stark effect for the bound Rydberg states of xenon. The extensive fine structure of xenon leads to spectra of great complexity which we have not been able to analyze in detail. Nonetheless, the major features of the spectra have been identified and a model of the p,d complex, showing substantial mixing even at low fields, is in fair agreement with observed energy levels. We expect to extend these measurements to the autoionizing Rydberg states in xenon, where the linewidths become another important parameter. An improved theoretical understanding of these results is certainly desirable.

ACKNOWLEDGMENTS

We wish to thank the Harvard-Smithsonian Center for Astrophysics for loan of the Channeltron detector. This work has been supported in part by grants from Research Corporation and The Ohio State University.

[1]R. F. Stebbings, C. J. Latimer, W. P. West, F. B. Dunning, and T. B. Cook, Phys. Rev. A **12**, 1453 (1975).
[2]C. Delsart, J.-C. Keller, and C. Thomas, J. Phys. B **14**, 4241 (1981).
[3]R. D. Knight and Liang-guo Wang, J. Opt. Soc. Am. B (to be published).
[4]J.-P. Grandin and X. Husson, J. Phys. B **14**, 433 (1981).
[5]P. Labastie, F. Biraben, and E. Giocobino, J. Phys. B **15**, 2595 (1982).
[6]B. E. Cole, J. W. Cooper, D. L. Ederer, G. Mehlman, and E. B. Saloman, J. Phys. B **13**, L175 (1980).
[7]Wallace L. Glab, G. B. Hillard, and Munir H. Nayfeh, Phys. Rev. A **28**, 3682 (1983).
[8]C. Delsart and J.-C. Keller, Phys. Rev. A **28**, 845 (1983).
[9]L. Minnhagen, Ark. Fys. **1**, 425 (1950).
[10]D. A. Harmin, Phys. Rev. A **26**, 2656 (1982); **30**, 2413 (1984).
[11]W. van de Water, D. R. Mariani, and P. M. Koch, Phys. Rev. A **30**, 2399 (1984).
[12]M. L. Zimmerman, M. G. Littman, M. M. Kash, and D. Kleppner, Phys. Rev. A **20**, 2251 (1979).
[13]M. L. Zimmerman, T. W. Ducas, M. G. Littman, and D. Kleppner, J. Phys. B **11**, L11 (1978).
[14]E. U. Condon and G. H. Shortley, *The Theory of Atomic Spectra* (Cambridge University, London, 1970).
[15]A. R. Edmonds, J. Picart, N. Tran Minh, and R. Pullen, J. Phys. B **12**, 2781 (1979).